Elastic Structure Preserving Impedance Control of Bidirectional Antagonistic Variable Stiffness Actuation

Xuming Meng, Manuel Keppler and Christian Ott

***Abstract*— We propose an impedance controller for articulated soft robots implemented by bidirectional antagonistic variable stiffness (BAVS) actuation, where two motors are connected via nonlinear elastic elements to a single link allowing for a joint stiffness modulation. Naturally, the highly elastic elements introduce undesired oscillatory dynamics into the plant. To address this problem, we present a controller that allows to impose a desired link-side stiffness and damping behavior while preserving the intrinsic inertial elastic properties of the system. This allows us to solve the global asymptotic regulation problem while simultaneously imposing a desired joint stiffness preset on the BAVS actuator. We provide a passivity and stability analysis based on a physically motivated storage and Lyapunov function. Experimental results on the underarm BAVS joint of DLR David validate our control law.**

I. Introduction

In recent years, soft robots or robots with compliant elements have attracted increasing attention. The soft-mechanism design enables the robot to attain natural dynamics [1], [2], energy-efficient locomotion [3], [4] or a safer human-robot-interaction in uncertain environments [5]–[7]. One category of the soft robots, whose structure comprises rigid parts (similar to skeletons) and compliant joints (generating analogous effects of muscles and tendons), have gained high popularity. They integrate a highly elastic element in the drive chain, e.g. Series Elastic Actuators (SEA) [8], Variable Stiffness Actuators (VSA) [9] [10] with advantages of large impact tolerance [10], low reflected inertia and energy storage for the explosive motions. As a consequence, numerous methods were developed for controlling such robots with elastic joints in terms of regulation or tracking tasks, e.g., PD-regulator with gravity compensation [11] [12], feedback linearization [13] [14], backstepping [15]. Recently, control methods based on inverse dynamics [16] and linear quadratic regulator [17] have been developed for VSA that allow the active variation of the mechanical stiffness. In [18] [19], passivity-based control laws are proposed and showed excellent performance for the impedance control on the robots with relatively stiff joints. However, the reduction of the joint stiffness by several magnitudes rendered previous state-of-the-art approaches not satisfactory. For those highly elastic robots, our previous work [21] introduced a passivity-based control approach to accomplish regulation and tracking tasks by injecting the damping directly on the link side, while the elastic structure of the plant is preserved. Later, we extended this work to an impedance controller, i.e., an Elastic Structure Preserving Impedance Control (ESπ-Control) [22], by implementing impedance control [23] for the Floating Spring Joints (FSJ) [10]. Experiments demonstrated good interaction performance with the environment for the joint-level and Cartesian impedance case. In [24], an extension of the ESP concept to Bidirectional Antagonistic Variables Stiffness (BAVS) is reported that solves the output regulation problem, while simultaneously allowing to adjust the passive stiffness of the joints. In this work, we generalize ESPπ controller to BAVS actuator, which are implemented in the forearm and the wrist of the elastic humanoid robot, David cf. Fig. 1. Compared to [24], the presented solution allows for greater freedom in shaping the interaction behavior of a BAVS actuator by allowing the implementation of a desired impedance behavior directly on the link.

The authors are with German Aerospace Center (DLR), Robotics and Mechatronics Center (RMC), Münchner Str. 20, 82234 Weßling, Germany (Email: xuming.meng@dlr.de)

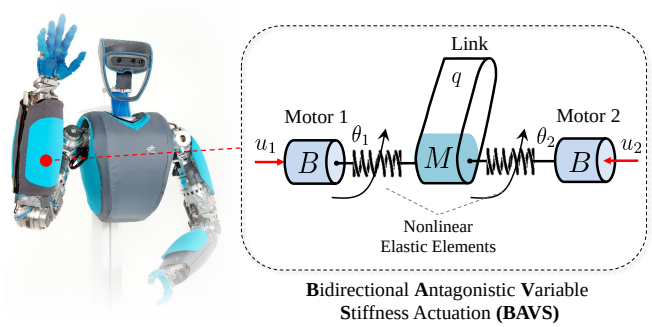

Fig. 1. The anthropomorphic robot David [20]. The forearm rotation joint and wrist joint are implemented with Bidirectional Antagonistic Variable Stiffness (BAVS) joints. A schematic diagram of the BAVS joint is depicted on the right.

In the following, this paper starts with an introduction to the working principle and characteristics of BAVS joints in Section II. In Section III to IV, the generalization of the ESπ controller with desired closed-loop link and motor dynamics is illustrated. Thereafter, analysis of the passivity and stability are discussed in Section V. At last, we present experimental results in Section VI that validate the proposed control in achieving a desired link-side compliance behavior.

II. Elastic Torque and Stiffness in BAVS Joints

The elastic humanoid robot David incorporates several different variable stiffness actuators [25]. The first four joints, namely three shoulder joints and one elbow joint, are implemented by FSJs [10]. Two motors of different sizes, with one adjusting the stiffness preset and the other providing torques on the link. For the remaining three joints

of the arm: the wrist (2-DoF) and the forearm rotation (1-DoF) are implemented by BAVS joints [26] [27] with more compact size compared to FSJs. Compared to the well-known antagonistic mechanism with positive tendon-force constraints [28], both motors of BAVS joints can either push or pull on the joint [26]. Figure 1 shows a simplified BAVS joint on the forearm rotation joint. The nonlinearity of the elastic element is achieved by a cam disc designed with a non-linear profile (not depicted here). The cam mechanism actuates a linear spring connected with one motor. Co-contracting the springs by the motors causes a change in stiffness, and asynchronous motion applies torque on the link [26]. The two motor coordinates are described by θ_i, with $i = 1, 2$. The link coordinate is represented by q, cf. Fig. 1. The general form of elastic torques and stiffness of the BAVS actuation is derived from a positive definite potential function $U_i(\theta_i - q) : \mathbb{R} \to \mathbb{R}^+$ for each of the two nonlinear elastic elements, which is assumed at least three times differentiable, and its gradient, the elastic torque $\tau_i : \mathbb{R} \to \mathbb{R}$ is a strictly monotonic increasing function, written as

$$\tau_i(\theta_i - q) := \frac{\partial U_i(\theta_i - q)}{\partial \theta_i} \ . \tag{1}$$

The link-side elastic torque $\psi : \mathbb{R}^2 \to \mathbb{R}$ is obtained from the elastic potential U_i as follows

$$\psi(\theta_1 - q, \theta_2 - q) := \sum_{i=1}^{2} \frac{\partial U_i(\theta_i - q)}{\partial q} = -\sum_{i=1}^{2} \frac{\partial U_i(\theta_i - q)}{\partial \theta_i} \ , \tag{2}$$

and, thus, can be rewritten as the superposition of the two elastic torques

$$\psi(\theta_1 - q, \theta_2 - q) = -\tau_1(\theta_1 - q) - \tau_2(\theta_2 - q) \tag{3}$$

The stiffness $k_i : \mathbb{R} \to \mathbb{R}^+$ is always positive, denoted as

$$k_i(\theta_i - q) := \frac{\partial \tau_i(\theta_i - q)}{\partial \theta_i} > 0 \ . \tag{4}$$

The physical link-side stiffness $\kappa : \mathbb{R}^2 \to \mathbb{R}$ is the gradient of the link-side torque ψ, given by

$$\kappa(\theta_1 - q, \theta_2 - q) := \frac{\partial \psi}{\partial q} = k_1(\theta_1 - q) + k_2(\theta_2 - q) \ . \tag{5}$$

The link-side torque and stiffness for David's forearm BAVS joint are depicted in Fig. 2. The pretension of a BAVS joint is determined by the motor position difference $\sigma = \theta_1 - \theta_2$. A detailed explanation can be found in [26]. The colored lines in top and bottom plots of Fig. 2 represent the feasible range of the link-side torque and stiffness when σ for three different pretension levels. The mechanical feasible range of the link-side torque ψ and stiffness κ is reduced with increasing σ. This features will be utilized in Section IV-B.

III. Control Objectives

The main goal of designing an ESπ controller is to let the soft robot achieve a desired compliant behavior when interacting with the human. We consider a model of 1-DoF robot dynamics with one BAVS joint integrated. It is assumed

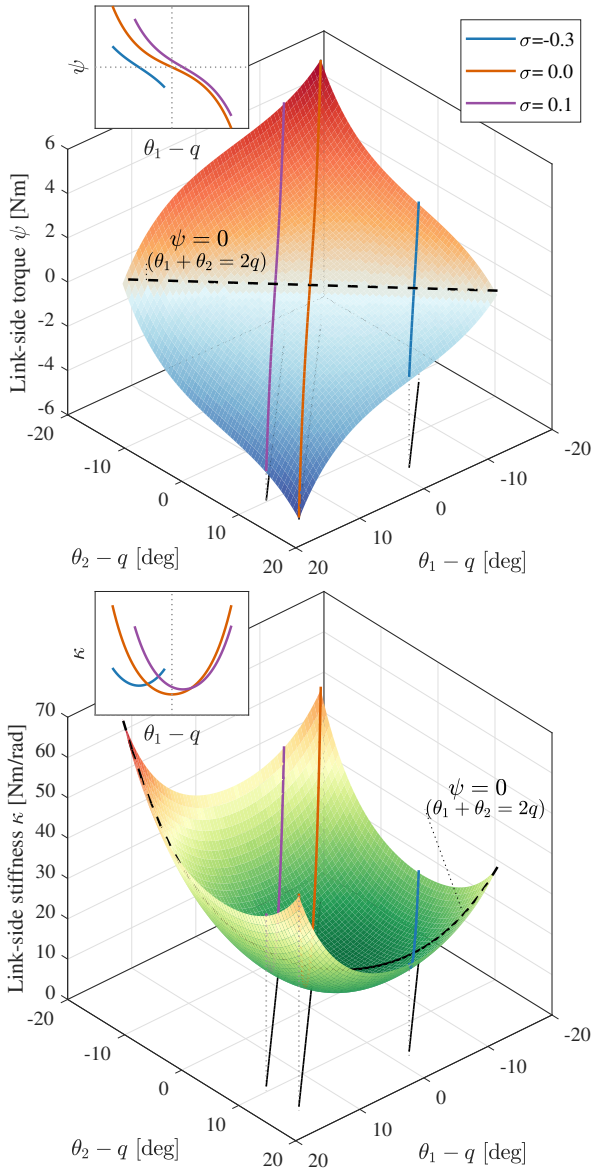

Fig. 2. The elastic torque ψ and local stiffness κ in two deflection coordinates $\theta_i - q$. The maximal deflection is $|\theta_i - q|_{max} = 15.5$ [deg]. The color lines represent the feasible region of ψ and κ, when the the motor coordinate difference, i.e., $\sigma = \theta_1 - \theta_2$ [rad] is set as a constant. The two small sub-figures depict ψ and κ with the corresponding σ in the coordinate $\theta_1 - q$ respectively. The blue line with the largest motor preset (absolute) value has the smallest feasible range of the torque and stiffness.

that the coupling effect of link inertia and motor inertia is neglectable, which is satisfied for e.g., highly geared motors [29]. The two motor coordinates and the link coordinate are described by θ_1, θ_2, and q, respectively. The actuator has two motors with identical inertia B which is coupled with the nonlinear elastic elements τ_1 and τ_2 to the link inertia M. The gravitational force $g(q)$ acts on the link side. The system dynamics together with (1) and (3) is written as

$$M\ddot{q} + g(q) + \psi(\theta_1 - q, \theta_2 - q) = \tau_{ext} \ , \tag{6}$$

$$B\ddot{\theta}_1 + \tau_1(\theta_1 - q) = u_1 \ , \tag{7}$$

$$B\ddot{\theta}_2 + \tau_2(\theta_2 - q) = u_2 \ , \tag{8}$$

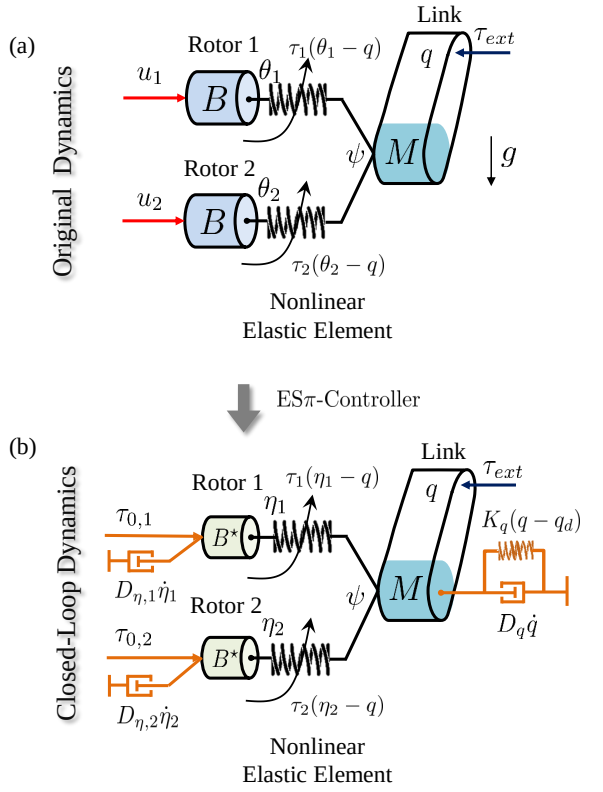

Fig. 3. Schematic diagram of a simplified single joint implemented with a BAVS joint in (a) the original dynamics and (b) the closed-loop dynamics achieved by implementing the ESπ controller.

where u_i is the i-th motor torque input, which serves as the control input. The original system dynamics is shown in Fig. 3(a). Only the motor coordinates θ_1 and θ_2 can be directly actuated by the physical motor inputs u_1, u_2. The link coordinate q can only be indirectly actuated by the link-side elastic torque ψ. Therefore, this form of under-actuation shows the major challenge in control of the state $(q, \dot{q})$.

Based on our aforementioned goal of the impedance controller, a desired closed-loop system dynamics is shown in Fig. 3(b). The target closed-loop dynamics can be expressed as

$$M\ddot{q} + D_q\dot{q} + K_q(q - q_d) + \psi(\eta_1 - q, \eta_2 - q) = \tau_{ext}, \quad (9)$$

$$B^\star\ddot{\eta}_1 + \tau_1(\eta_1 - q) = \tau_{0,1} - D_{\eta,1}\dot{\eta}_1, \quad (10)$$

$$B^\star\ddot{\eta}_2 + \tau_2(\eta_2 - q) = \tau_{0,2} - D_{\eta,2}\dot{\eta}_2, \quad (11)$$

$$\psi(\eta_1 - q, \eta_2 - q) = -\tau_1(\eta_1 - q) - \tau_2(\eta_2 - q). \quad (12)$$

Firstly, we obtain a desired closed-loop link-side dynamics (9) by adding a spring K_q and a positive damping D_q[1] to the original link inertia M, cf. Fig. 3(b). The link-side equilibrium is given by $q = q_d, \dot{q} = 0$. In (12), the virtual link-side elastic torque ψ has an identical form with (3) in the original physical system. It is important to notice that the desired dynamics utilizes a different set of motor coordinates, i.e., η_i instead of θ_i, such that the virtual link-side torque ψ is also based on these coordinates. The transformation from the old motor coordinate θ_i to the new virtual coordinate η_i will be concretely illustrated in Section IV-A. One can shape the physical motor inertia from B to a scaled-down inertia $B^\star$ [19]. Meanwhile, the link-side stiffness behavior of the closed-loop system, defined by $\frac{\Delta\tau_{ext}}{\Delta q}\Big|_{\substack{\dot{q}=0\\ \dot{\eta}_i=0}}$, should equal the demanded stiffness K_q. Secondly, we add two positive damper terms $D_{\eta,i}$ on the motor side to suppress the oscillation. Finally, we add additionally two constant feed-forward terms $\tau_{0,1}$ and $\tau_{0,2}$ for generating internal torques. We require that change of the motor pretension should not affect the desired link-side closed-loop dynamics (9). Thus, the relation

$$\tau_{0,1} + \tau_{0,2} = 0\ , \quad (13)$$

should be always fulfilled. We summarize the system state vector in $\boldsymbol{z} = \begin{bmatrix} q & \eta_1 & \eta_2 & \dot{q} & \dot{\eta}_1 & \dot{\eta}_2 \end{bmatrix}^T$. The unique system equilibrium when $\tau_{ext} = 0$ is given by

$$\boldsymbol{z}_{eq} = \begin{bmatrix} q_d & \eta_{1,d} & \eta_{2,d} & 0 & 0 & 0 \end{bmatrix}^T. \quad (14)$$

IV. Controller Design

In this section, achieving the desired closed-loop dynamics (9)(10)(11) from the original system dynamics (6)(7)(8) is illustrated. Firstly, the coordinate transformation from the original motor coordinate θ_i to the new virtual coordinate η_i is introduced. In the following text, we use $\bar{(\cdot)}$ notation to represent the function which has identical formulation with the old one $(\cdot)$ but now written with the new argument η_i.

A. Coordinate Transformation

By comparing (9) to (6), we get

$$\psi(\theta_1 - q, \theta_2 - q) := \bar{\psi}(\eta_1 - q, \eta_2 - q) - \underbrace{(g(q) - K_q(q - q_d) - D_q\dot{q})}_{:=\tau_d}\ , \quad (15)$$

where the term $g(q)$ cancels the effect of the gravity. In fact, τ_d has the same form as a classic impedance controller with gravity compensation for rigid-body robots. The new motor coordinates η_1 and η_2 reflect the desired link behavior. However, by imposing only (15), there is an infinite number of solutions for the two virtual motor coordinates. For a unique mapping from the old coordinate θ_i to the new one η_i for both motors, an additional constraint is required. Theoretically, we can arbitrarily design a constraint to obtain the unique solution of η_i. In Section II, we have mentioned that the motor stiffness preset $\sigma = \theta_1 - \theta_2$ has physical meaning for altering the motor pretension. Inspired by that, we impose a simple kinematic constraint in the form

$$\eta_1 - \eta_2 := \theta_1 - \theta_2\ , \quad (16)$$

i.e., the difference of new coordinates should be the same as the old one. Therefore, the new coordinate η_1 and η_2 can be uniquely determined from (15) and (16). Next, having the

[1]We assume K_q and D_q to be constant for simplicity.

time derivative of (15) and (16), the velocity of the original motor coordinate is written as

$$\underbrace{\begin{bmatrix}\dot\theta_1\\ \dot\theta_2\end{bmatrix}}_{\dot{\boldsymbol\theta}} = \begin{bmatrix}\frac{\partial\psi}{\partial\theta_1} & \frac{\partial\psi}{\partial\theta_2}\\ 1 & -1\end{bmatrix}^{-1}\Bigg(\begin{bmatrix}\frac{\partial\bar\psi}{\partial\eta_1} & \frac{\partial\bar\psi}{\partial\eta_2}\\ 1 & -1\end{bmatrix}\underbrace{\begin{bmatrix}\dot\eta_1\\ \dot\eta_2\end{bmatrix}}_{\dot{\boldsymbol\eta}} + \begin{bmatrix}\frac{\partial\bar\psi}{\partial q}\dot q - \frac{\partial\psi}{\partial q}\dot q - \dot\tau_d\\ 0\end{bmatrix}\Bigg) . \tag{17}$$

We take time derivative of (17) again to obtain acceleration

$$\underbrace{\begin{bmatrix}\ddot\theta_1\\ \ddot\theta_2\end{bmatrix}}_{\ddot{\boldsymbol\theta}} = \underbrace{\begin{bmatrix}\frac{\partial\psi}{\partial\theta_1} & \frac{\partial\psi}{\partial\theta_2}\\ 1 & -1\end{bmatrix}^{-1}\begin{bmatrix}\frac{\partial\bar\psi}{\partial\eta_1} & \frac{\partial\bar\psi}{\partial\eta_2}\\ 1 & -1\end{bmatrix}}_{\boldsymbol A}\underbrace{\begin{bmatrix}\ddot\eta_1\\ \ddot\eta_2\end{bmatrix}}_{\ddot{\boldsymbol\eta}} + \underbrace{\begin{bmatrix}\frac{\partial\psi}{\partial\theta_1} & \frac{\partial\psi}{\partial\theta_2}\\ 1 & -1\end{bmatrix}^{-1}\begin{bmatrix}c_1 + \frac{\partial\bar\psi}{\partial q}\ddot q - c_2 - \frac{\partial\psi}{\partial q}\ddot q - \ddot\tau_d\\ 0\end{bmatrix}}_{\boldsymbol a} , \tag{18}$$

where the terms c_1 and c_2 are given by

$$c_1 = \begin{bmatrix}\frac{\partial^2\bar\psi}{\partial\eta_1^2}\dot\eta_1 + \frac{\partial^2\bar\psi}{\partial\eta_1\partial\eta_2}\dot\eta_2 + \frac{\partial^2\bar\psi}{\partial\eta_1\partial q}\dot q\\ \frac{\partial^2\bar\psi}{\partial\eta_1\partial\eta_2}\dot\eta_1 + \frac{\partial^2\bar\psi}{\partial\eta_2^2}\dot\eta_2 + \frac{\partial^2\bar\psi}{\partial\eta_2\partial q}\dot q\\ \frac{\partial^2\bar\psi}{\partial\eta_1\partial q}\dot\eta_1 + \frac{\partial^2\bar\psi}{\partial\eta_2\partial q}\dot\eta_2 + \frac{\partial^2\bar\psi}{\partial q^2}\dot q\end{bmatrix}^T\begin{bmatrix}\dot\eta_1\\ \dot\eta_2\\ \dot q\end{bmatrix} , \tag{19}$$

$$c_2 = \begin{bmatrix}\frac{\partial^2\psi}{\partial\theta_1^2}\dot\theta_1 + \frac{\partial^2\psi}{\partial\theta_1\partial\theta_2}\dot\theta_2 + \frac{\partial^2\psi}{\partial\theta_1\partial q}\dot q\\ \frac{\partial^2\psi}{\partial\theta_1\partial\theta_2}\dot\theta_1 + \frac{\partial^2\psi}{\partial\theta_2^2}\dot\theta_2 + \frac{\partial^2\psi}{\partial\theta_2\partial q}\dot q\\ \frac{\partial^2\psi}{\partial\theta_1\partial q}\dot\theta_1 + \frac{\partial^2\psi}{\partial\theta_2\partial q}\dot\theta_2 + \frac{\partial^2\psi}{\partial q^2}\dot q\end{bmatrix}^T\begin{bmatrix}\dot\theta_1\\ \dot\theta_2\\ \dot q\end{bmatrix} , \tag{20}$$

respectively. Therefore, the relations (15)-(18) lead to a motor coordinate transformation for the motor dynamics (7)(8), written in matrix-form

$$\underbrace{\begin{bmatrix}B & 0\\ 0 & B\end{bmatrix}}_{\boldsymbol B}\underbrace{\left(\boldsymbol A\begin{bmatrix}\ddot\eta_1\\ \ddot\eta_2\end{bmatrix} + \boldsymbol a\right)}_{\ddot{\boldsymbol\theta}} + \underbrace{\begin{bmatrix}\tau_1(\theta_1,q)\\ \tau_2(\theta_2,q)\end{bmatrix}}_{\boldsymbol\tau} = \underbrace{\begin{bmatrix}u_1\\ u_2\end{bmatrix}}_{\boldsymbol u} \tag{21}$$

Now, the control input is chosen as

$$\boldsymbol u = \boldsymbol B\boldsymbol a + \boldsymbol\tau - \boldsymbol B\boldsymbol A\boldsymbol B^{\star-1}\Bigg(\underbrace{\begin{bmatrix}\bar\tau_1\\ \bar\tau_2\end{bmatrix}}_{\bar{\boldsymbol\tau}} + \boldsymbol D_\eta\dot{\boldsymbol\eta} - \underbrace{\begin{bmatrix}\bar\tau_{0,1}\\ \bar\tau_{0,2}\end{bmatrix}}_{\bar{\boldsymbol\tau}_0}\Bigg) , \tag{22}$$

where $\boldsymbol D_\eta = diag(D_{\eta,1}, D_{\eta,2}) \in \mathbb{R}^{2\times2}$ is a positive definite diagonal damping matrix, and $\bar{\boldsymbol\tau}_0$ is a constant internal torque term for setting motor pretension. The diagonal matrix $\boldsymbol B^\star = \beta\boldsymbol B$ is the scaled motor inertia. Generally, the scaling factor is chosen by $\beta \in (0, 1]$. The motor inertia shaping can be regarded as linear amplification of feedback signals, i.e., the virtual spring torque $\bar{\boldsymbol\tau}$ and motor-side damping term $\boldsymbol D_\eta$. Therefore, by giving (22), the desired closed-loop system dynamics (9)-(11) is achieved.

B. Setting Motor Pretension by σ_d and q_d

We can use desired motor stiffness preset σ_d for achieving a desired motor pretension. Substitute the system equilibrium (14) into (10)(11), the feedforward terms can be uniquely determined by

$$\bar\tau_{0,1} = \bar\tau_1(\eta_{1,d} - q_d) , \tag{23}$$

$$\bar\tau_{0,2} = \bar\tau_2(\eta_{2,d} - q_d) . \tag{24}$$

Substitute (23)(24) into (13), we get

$$\bar\psi_0(\eta_{1,d} - q_d, \eta_{2,d} - q_d) = \bar\tau_{0,1} + \bar\tau_{0,2} = 0 . \tag{25}$$

By solving (25), we have

$$\eta_{1,d} + \eta_{2,d} = 2q_d . \tag{26}$$

Now, we want the two virtual motor coordinates to hold a constant σ_d,

$$\eta_{1,d} - \eta_{2,d} = \sigma_d . \tag{27}$$

which is equivalent to $\theta_1 - \theta_2 = \sigma_d$, due to (16). By solving for η_1 and η_2 with (26) and (27), the equilibrium of virtual motor coordinates $\eta_{1,d}$ and $\eta_{2,d}$ are now written as functions of σ_d and q_d

$$\eta_{1,d} = q_d + \frac{1}{2}\sigma_d , \tag{28}$$

$$\eta_{2,d} = q_d - \frac{1}{2}\sigma_d . \tag{29}$$

As we mentioned at the beginning of this section, by just replacing θ_i with η_i in (3) and (5), we get the virtual torque and stiffness profiles in the new coordinate, since the virtual elastic torque $\bar\psi$ shares the same formulation with the physical ψ, cf. Fig. 2. Thus, the solution (26) can be represented by the black dashed line in Fig. 2 as well. The location of the intersection point, e.g., where the purple line and the black dashed line intersects, denotes the equilibrium (14) of the closed-loop system when we command stiffness preset $\sigma_d = 0.1$ [rad].

C. Achieving Desired Link-side Stiffness

By introducing the new virtual coordinate η_i, the link-side stiffness $\frac{\Delta\tau_{ext}}{\Delta q}\Big|_{\substack{q=q_d\\ \dot q=0\\ \dot\eta_i=0}}$ should be equal to the commanded K_q. The proof is shown is the following:

Proof. A constant external force $\tau_{ext} \neq 0$ is now acting on the link side of a stable closed-loop system , the system has a new stable state $(q = q^*, \eta_1 = \eta_1^*, \eta_2 = \eta_2^*, \dot q = \ddot q = 0, \dot\eta_i = \ddot\eta_i = 0)$. Substitute the new state into (9), we have

$$K_q(q^* - q_d) + \bar\psi(\eta_1^* - q^*, \eta_2^* - q^*) = \tau_{ext} . \tag{30}$$

Since the motor pretension $\bar\tau_{0,1}$ and $\bar\tau_{0,2}$ still hold constant, the link-side torque $\bar\psi$ still holds the relation in (25), i.e.,

$$\bar\psi(\eta_1^* - q^*, \eta_2^* - q^*) = 0 . \tag{31}$$

Thus, by substituting (31) into (30), we have

$$K_q(q^* - q_d) = \tau_{ext} . \tag{32}$$

We finally substitute $\Delta q = q^* - q_d$ and $\Delta\tau_{ext} = \tau_{ext} - 0$ in (32), we get

$$\frac{\Delta\tau_{ext}}{\Delta q} = K_q \ . \tag{33}$$

□

V. Passivity and Stability Analysis

A. Passivity

In the following, the passivity property of the closed-loop system with the external human interaction forces $\tau_{ext} \neq 0$ is analyzed. Following the physical design approach, we can use energy-based storage functions for the link and motor dynamics (9)-(11) with respect to the reference dynamics, formulated as

$$S_q = \frac{1}{2}M\dot{q}^2 + \frac{1}{2}K_q(q - q_d)^2 \ , \tag{34}$$

$$S_\eta = \frac{1}{2}B\dot{\eta}_1^2 + \frac{1}{2}B\dot{\eta}_2^2 + \bar{U}(\tilde{\eta}_1, \tilde{\eta}_2, \tilde{q}) \ , \tag{35}$$

where $\bar{U}(\tilde{\eta}_1, \tilde{\eta}_2, \tilde{q})$ is the potential energy difference written in the deviation coordinate. The deviation terms are defined by $\tilde{\eta}_i := \eta_i - \eta_{i,d}$ and $\tilde{q} := q - q_d$. The total virtual kinetic and potential energy of the closed-loop system is written in $S = S_q + S_\eta$. The time derivatives of the storage function is formulated as

$$\dot{S}_q = \dot{q}\tau_{ext} - D_q\dot{q}^2 + \bar{\psi}\dot{q} \ , \tag{36}$$

$$\begin{aligned}\dot{S}_\eta &= \dot{q}\bar{\tau}_{0,1} + \dot{q}\bar{\tau}_{0,2} - D_{\eta,1}\dot{\eta}_1^2 - D_{\eta,2}\dot{\eta}_2^2 - \bar{\psi}\dot{q} \\ &= -D_{\eta,1}\dot{\eta}_1^2 - D_{\eta,2}\dot{\eta}_2^2 - \bar{\psi}\dot{q} \ ,\end{aligned} \tag{37}$$

where $\bar{\psi}\dot{q}$ represents the power exchange within the motor and the link dynamics, and $\dot{q}\tau_{ext}$ reflects an external power-interconnection between the system and the environment. Due to (13), the two feedforward terms are always canceled, i.e., $\dot{q}\bar{\tau}_{0,1} + \dot{q}\bar{\tau}_{0,2} = 0$.

Proposition 1. *The closed-loop system* (9)-(11) *represents a passive map from external force τ_{ext} to the velocity $\dot{q}$.*

Proof. The time derivatives of the closed-loop system yields to

$$\dot{S}_q + \dot{S}_\eta = \dot{q}\tau_{ext} - D_{\eta,1}\dot{\eta}_1^2 - D_{\eta,2}\dot{\eta}_2^2 - D_q\dot{q}^2 \leq \dot{q}\tau_{ext} \ . \tag{38}$$

□

B. Stability

In this section, the stability analysis of the closed-loop system (9)-(11) with free motion $\tau_{ext} = 0$ is introduced.

Proposition 2. *The equilibrium point* (14) *of the closed-loop system, in absence of external force τ_{ext}, is globally asymptotically stable.*

Proof. Choose the Lyapunov function candidate with the same storage function $V(\boldsymbol{z}) = S$, which is a positive definite function. Its time derivative is given by

$$\dot{V} = -D_{\eta,1}\dot{\eta}_1^2 - D_{\eta,2}\dot{\eta}_2^2 - D_q\dot{q}^2 \leq 0 \ , \tag{39}$$

which is a negative semi-definite function. With LaSalle's invariance principle, $\dot{V} = 0$ can be achieved only if $q = q_d$, $\eta_1 = \eta_{1,d}$, $\eta_2 = \eta_{2,d}$, $\dot{\eta}_1 = \dot{\eta}_2 = \dot{q} = 0$. Furthermore, if the state vector $||\boldsymbol{z}|| \to \infty$, the storage function is then radially unbounded, i.e., $V(\boldsymbol{z}) \to \infty$. The system equilibrium (14) is thus globally asymptotically stable. □

VI. Experiments

In this section, we present an experiment for validation of the proposed impedance controller when the human interacts with the system. The experiment is performed on the rotation axis of the forearm of David robot, with a BAVS joint integrated. The experiment setup is shown in Fig. 4. The modal damping factors ξ_q and ξ_η of the link and the motors are chosen in a similar way with [30] for the design of damping factors $D_q = 2\xi_q\sqrt{K_q M}$ and $D_{\eta,i} = 2\xi_\eta\sqrt{\bar{k}_i B^\star}$, where $\bar{k}_i$ is the stiffness written in the new coordinate η_i. A motor friction observer [31] [32] is implemented during all trails. The user exerts the torque on the link, cf. Fig. 5. The external force τ_{ext} is estimated by a momentum based observer [32]. By varying K_q from 5 to 50 [Nm/rad], we conducted the experiments with two stiffness presets $\sigma_d = 0.1$ [rad] and $\sigma_d = 0.3$ [rad], respectively. All parameters are summarized in Tab. I. Note that, the larger stiffness preset σ_d is, the lower peak external torque τ_{ext} the human interaction force can reach. It is due to the feasible range of the link-side elastic torque is reduced by increasing motor stiffness preset as well, e.g., compare the maximal torques between the stiffness preset $\sigma_d = 0$ [rad] (the red line) and $\sigma_d = 0.1$ [rad] (the purple line) in Fig. 2. During the experiments, the physical link stiffness κ is recorded at the same time, cf. Fig. 7.

The relation between the external force τ_{ext} and the link-side error $\tilde{q}$ is depicted in Fig. 6. The link-side stiffness $\frac{\Delta\tau_{ext}}{\Delta\tilde{q}}$ (colored and gray lines) is approximated by the ramp of a linear regression model (black dashed lines). The comparison

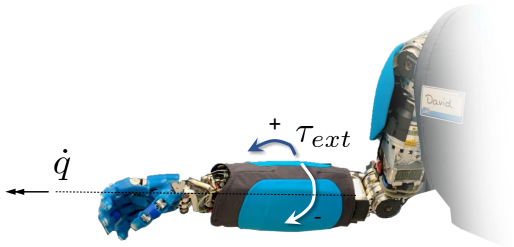

Fig. 4. Experiment setup for the impedance behavior w.r.t. the human interaction. The forearm of the elastic robot David in the initial configuration $q = q_d$. The other joints (shoulder and elbow) are controlled with our previous ESP-Controller [30] to avoid unnecessary oscillations from other joints.

TABLE I
Parameters of Controller

No.	K_q [Nm rad^{-1}]	σ_d [rad]	ξ_q	ξ_η	β
1	5	0.1/0.3	0.5	0.1	0.3
2	15	0.1/0.3	0.5	0.1	0.3
3	25	0.1/0.3	0.5	0.1	0.3
4	50	0.1/0.3	0.5	0.1	0.3

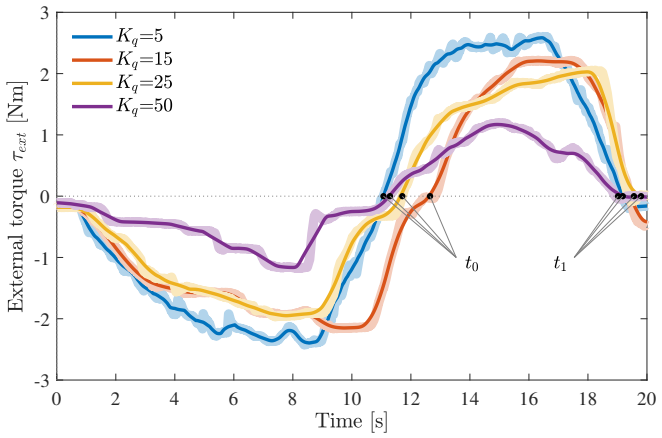

Fig. 5. Estimated external torque τ_{ext} acts on the BAVS joint, when the commanded $\sigma_d = 0.3$ [rad]. The color lines represent the filtered estimated external torque with corresponding commanded K_q. The two time points t_0 and t_1 for each trail are defined by the start and end time when the external force τ_{ext} is in a positive period.

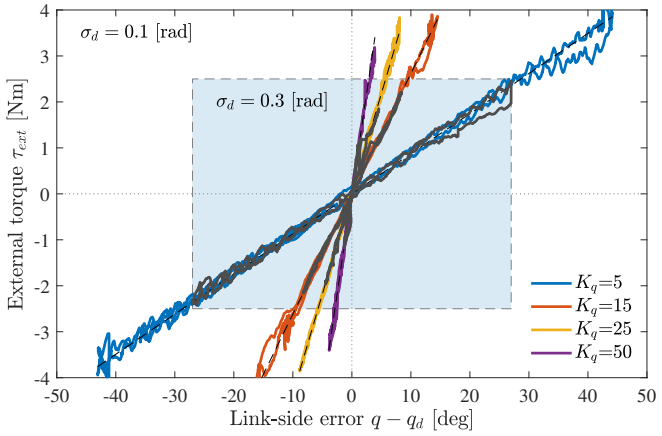

Fig. 6. External torque τ_{ext} vs. link deflection $\tilde{q} = q - q_d$. The color lines represents the external torque with different commanded K_q, when the stiffness preset is $\sigma_d = 0.1$ [rad]. The gray lines in the blue area denote the trails when the stiffness preset is $\sigma_d = 0.3$ [rad]. The stiffness preset only affects the feasible range of the link deflection (or maximal allowable external torque). Hence, it can be concluded that the desired link-side stiffness is obtained.

of commanded K_q and the actual stiffness are summarized in Tab. II. The low relative errors verify our first conclusion: The link side stiffness K is only determined by the stiffness setting K_q in the impedance controller and is independent from the physical joint stiffness κ. In addition, the feasible range of the link-side error $\tilde{q}$ is constrained by the stiffness preset value σ_d, e.g., the gray lines (with $\sigma_d = 0.3$ [rad]) in the blue area of Fig. 6 show a smaller feasible range of the link. Figure 7 depicts the different stiffness value when commanded K_q is changed. The second conclusion we have is that the link-side stiffness K_q could either be smaller or even larger than the physical joint stiffness κ (e.g., ca. 3 times larger in the case: $K_q = 50$ [Nm/rad] and $\sigma_d = 0.3$ [rad]). What's more, σ_d restricts the maximal range of the physical joint stiffness κ, cf. the amplitude difference of color lines in the upper and the bottom plot in Fig. 7.

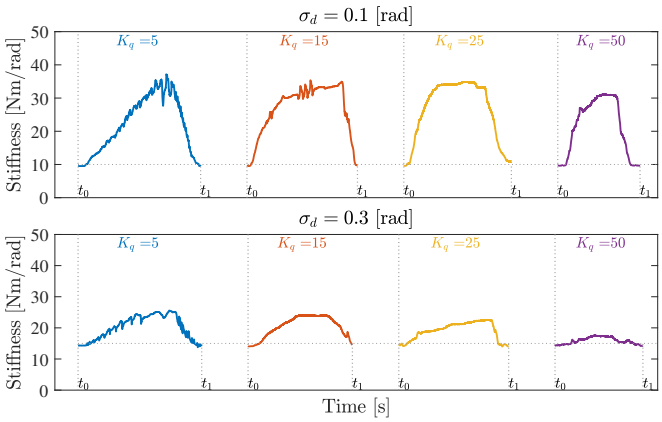

Fig. 7. Comparison of the physical stiffness $\kappa(\theta_1 - q, \theta_2 - q)$ and commanded stiffness K_q. Four stiffness curves with two different preset are shown on the top ($\sigma_d = 0.1$ [rad]) and the bottom ($\sigma_d = 0.3$ [rad]) plot respectively. The selected time interval is defined in Fig. 5.

TABLE II

RESULTS OF LINK-SIDE BEHAVIOR

commanded K_q [Nm rad^{-1}]	commanded σ_d [rad]	$\frac{\Delta\tau_{ext}}{\Delta\tilde{q}}$	relative error
5	0.1	4.9	-2.0%
15	0.1	15.1	0.6%
25	0.1	25.1	0.4%
50	0.1	49.1	-1.8%
5	0.3	4.9	-2.0%
15	0.3	14.9	-0.6%
25	0.3	24.5	-2.0%
50	0.3	49.6	-0.8%

VII. CONCLUSIONS

This paper presents an impedance control concept for soft robots with Bidirectional Antagonistic Variable Stiffness (BAVS) actuators integrated with nonlinear elastic elements. Following the ESπ control framework from [22], the desired impedance behavior has been achieved by the proposed controller that enables to impose a desired link-side stiffness and damping behavior directly on the link side. Meanwhile, the inertial properties and the elastic structure of the system are preserved. To achieve the desired motor pretension, two constant internal torques, which have the same amplitude but with opposite signs, have been designed by giving the desired link-side equilibrium and the desired motor position difference for both BAVS motors. In this way, the change of motor stiffness preset will not lead to the variation of the link-side torque. Besides, a damping term is added on the motor side to suppress the undesired oscillation. We provided a stability and passivity analysis based on a physically motivated storage function. The experimental results showed satisfactory compliance behavior with respect to human interaction. In the future, the control concept will be extended to David's wrist, implemented by two BAVS joints with more complex internal motor torque coupling. Besides, an extension to a multi-DoF robot will also be our future work. We hope this concept can be implemented in further applications of nonlinear elastic robots.

REFERENCES

[1] T. McGeer, "Passive dynamic walking," *The International Journal of Robotics Research*, vol. 9, no. 2, pp. 62–82, apr 1990. doi: 10.1177/027836499000900206

[2] B. Vanderborght, B. Verrelst, R. V. Ham, M. V. Damme, D. Lefeber, B. M. Y. Duran, and P. Beyl, "Exploiting natural dynamics to reduce energy consumption by controlling the compliance of soft actuators," *The International Journal of Robotics Research*, vol. 25, no. 4, pp. 343–358, apr 2006. doi: 10.1177/0278364906064566

[3] W. Xi and C. D. Remy, "Optimal gaits and motions for legged robots," in *2014 IEEE/RSJ International Conference on Intelligent Robots and Systems*. IEEE, sep 2014. doi: 10.1109/iros.2014.6943015

[4] G. A. Folkertsma and S. Stramigioli, "Energy in robotics," *Foundations and Trends in Robotics*, vol. 6, no. 3, pp. 140–210, 2017. doi: 10.1561/2300000038

[5] K. Laurin-Kovitz, J. Colgate, and S. Carnes, "Design of components for programmable passive impedance," in *Proceedings. 1991 IEEE International Conference on Robotics and Automation*. IEEE Comput. Soc. Press, 1991. doi: 10.1109/robot.1991.131824

[6] M. Zinn, O. Khatib, and B. Roth, "A new actuation approach for human friendly robot design," in *IEEE International Conference on Robotics and Automation, 2004. Proceedings. ICRA '04. 2004.* IEEE, 2004. doi: 10.1109/robot.2004.1307159

[7] A. Bicchi, M. A. Peshkin, and J. E. Colgate, "Safety for physical human–robot interaction," in *Springer Handbook of Robotics*. Springer Berlin Heidelberg, 2008, pp. 1335–1348.

[8] G. Pratt and M. Williamson, "Series elastic actuators," in *Proceedings 1995 IEEE/RSJ International Conference on Intelligent Robots and Systems. Human Robot Interaction and Cooperative Robots*. IEEE Comput. Soc. Press. doi: 10.1109/iros.1995.525827

[9] G. Tonietti, R. Schiavi, and A. Bicchi, "Design and control of a variable stiffness actuator for safe and fast physical human/robot interaction," in *Proceedings of the 2005 IEEE International Conference on Robotics and Automation*. IEEE, 2005. doi: 10.1109/robot.2005.1570172

[10] S. Wolf, O. Eiberger, and G. Hirzinger, "The DLR FSJ: Energy based design of a variable stiffness joint," in *2011 IEEE International Conference on Robotics and Automation*. IEEE, may 2011. doi: 10.1109/icra.2011.5980303

[11] P. Tomei, "Adaptive PD controller for robot manipulators," *IEEE Transactions on Robotics and Automation*, vol. 7, no. 4, pp. 565–570, 1991. doi: 10.1109/70.86088

[12] A. D. Luca and F. Flacco, "A PD-type regulator with exact gravity cancellation for robots with flexible joints," in *2011 IEEE International Conference on Robotics and Automation*. IEEE, may 2011. doi: 10.1109/icra.2011.5979615

[13] A. de Luca and P. Lucibello, "A general algorithm for dynamic feedback linearization of robots with elastic joints," in *Proceedings. 1998 IEEE International Conference on Robotics and Automation (Cat. No.98CH36146)*. IEEE, 1998. doi: 10.1109/robot.1998.677024

[14] G. Buondonno and A. D. Luca, "Efficient computation of inverse dynamics and feedback linearization for VSA-based robots," *IEEE Robotics and Automation Letters*, vol. 1, no. 2, pp. 908–915, jul 2016. doi: 10.1109/lra.2016.2526072

[15] P. Kokotovic, M. Krstic, and I. Kanellakopoulos, "Backstepping to passivity: recursive design of adaptive systems," in *Proceedings of the 31st IEEE Conference on Decision and Control*. IEEE, 1992. doi: 10.1109/cdc.1992.371031

[16] H. Chang, S. J. Kim, and J. Kim, "Feedforward motion control with a variable stiffness actuator inspired by muscle cross-bridge kinematics," *IEEE Transactions on Robotics*, vol. 35, no. 3, pp. 747–760, jun 2019. doi: 10.1109/tro.2019.2900567

[17] L. Liu, S. Leonhardt, C. Ngo, and B. J. E. Misgeld, "Impedance-controlled variable stiffness actuator for lower limb robot applications," *IEEE Transactions on Automation Science and Engineering*, vol. 17, no. 2, pp. 991–1004, apr 2020. doi: 10.1109/tase.2019.2954769

[18] C. Ott, A. Albu-Schäffer, A. Kugi, and G. Hirzinger, "Decoupling based cartesian impedance control of flexible joint robots," in *2003 IEEE International Conference on Robotics and Automation (Cat. No.03CH37422)*. IEEE, 2003. doi: 10.1109/robot.2003.1242067

[19] ——, "On the passivity-based impedance control of flexible joint robots," *IEEE Transactions on Robotics*, vol. 24, no. 2, pp. 416–429, apr 2008. doi: 10.1109/tro.2008.915438

[20] A. Albu-Schäffer, O. Eiberger, M. Fuchs, M. Grebenstein, S. Haddadin, C. Ott, A. Stemmer, T. Wimböck, S. Wolf, C. Borst, and G. Hirzinger, "Anthropomorphic soft robotics – from torque control to variable intrinsic compliance," in *Springer Tracts in Advanced Robotics*. Springer Berlin Heidelberg, 2011, pp. 185–207.

[21] M. Keppler, D. Lakatos, C. Ott, and A. Albu-Schäffer, "Elastic structure preserving (ESP) control for compliantly actuated robots," *IEEE Transactions on Robotics*, vol. 34, no. 2, pp. 317–335, apr 2018. doi: 10.1109/tro.2017.2776314

[22] ——, "Elastic structure preserving impedance (ESπ)control for compliantly actuated robots," in *2018 IEEE/RSJ International Conference on Intelligent Robots and Systems (IROS)*. IEEE, oct 2018. doi: 10.1109/iros.2018.8593415

[23] N. Hogan, "Impedance control: An approach to manipulation: Part i—theory," *Journal of Dynamic Systems, Measurement, and Control*, vol. 107, no. 1, pp. 1–7, mar 1985. doi: 10.1115/1.3140702

[24] R. Mengacci, M. Keppler, M. Pfanne, A. Bicchi, and C. Ott, "Elastic structure preserving control for compliant robots driven by agonistic-antagonistic actuators (ESPaa)," *IEEE Robotics and Automation Letters*, vol. 6, no. 2, pp. 879–886, apr 2021. doi: 10.1109/lra.2021.3052434

[25] M. Grebenstein, A. Albu-Schäffer, T. Bahls, M. Chalon, O. Eiberger, W. Friedl, R. Gruber, S. Haddadin, U. Hagn, R. Haslinger, H. Hoppner, S. Jorg, M. Nickl, A. Nothhelfer, F. Petit, J. Reill, N. Seitz, T. Wimbock, S. Wolf, T. Wusthoff, and G. Hirzinger, "The DLR hand arm system," in *2011 IEEE International Conference on Robotics and Automation*. IEEE, may 2011. doi: 10.1109/icra.2011.5980371

[26] W. Friedl, H. Hoppner, F. Petit, and G. Hirzinger, "Wrist and forearm rotation of the DLR hand arm system: Mechanical design, shape analysis and experimental validation," in *2011 IEEE/RSJ International Conference on Intelligent Robots and Systems*. IEEE, sep 2011.

[27] F. Petit, M. Chalon, W. Friedl, M. Grebenstein, A. Albu-Schäffer, and G. Hirzinger, "Bidirectional antagonistic variable stiffness actuation: Analysis, design & implementation," in *2010 IEEE International Conference on Robotics and Automation*. IEEE, may 2010. doi: 10.1109/robot.2010.5509267

[28] K. Koganezawa, Y. Watanabe, and N. Shimizu, "Antagonistic muscle-like actuator and its application to multi-d.o.f. forearm prosthesis," *Advanced Robotics*, vol. 12, no. 7-8, pp. 771–789, jan 1997. doi: 10.1163/156855399x00135

[29] M. W. Spong, "Modeling and control of elastic joint robots," *Journal of Dynamic Systems, Measurement, and Control*, vol. 109, no. 4, pp. 310–318, dec 1987. doi: 10.1115/1.3143860

[30] M. Keppler, D. Lakatos, C. Ott, and A. Albu-Schäffer, "A passivity-based approach for trajectory tracking and link-side damping of compliantly actuated robots," in *2016 IEEE International Conference on Robotics and Automation (ICRA)*. IEEE, may 2016. doi: 10.1109/icra.2016.7487239

[31] A. D. Luca and R. Mattone, "Actuator failure detection and isolation using generalized momenta," in *2003 IEEE International Conference on Robotics and Automation (Cat. No.03CH37422)*. IEEE, 2003. doi: 10.1109/robot.2003.1241665

[32] A. D. Luca, A. Albu-Schäffer, S. Haddadin, and G. Hirzinger, "Collision detection and safe reaction with the DLR-III lightweight manipulator arm," in *2006 IEEE/RSJ International Conference on Intelligent Robots and Systems*. IEEE, oct 2006. doi: 10.1109/iros.2006.282053